

RESEARCH

Open Access



Differentiation of adipose-derived stem cells to functional CD105^{neg} CD73^{low} melanocyte precursors guided by defined culture condition

Gabriela Zavala^{1,4}, Carolina Sandoval⁴, Daniel Meza^{1,4}, Rafael Contreras^{3,4}, Walter Gubelin⁵ and Maroun Khoury^{1,2,3,4*}

Abstract

Background: The generation of functional human epidermal melanocytes (HEM) from stem cells provides an unprecedented source for cell-based therapy in vitiligo. Despite the important efforts exerted to obtain melanin-producing cells from stem cells, pre-clinical results still lack the safety and scalability characteristics essential for their translational application.

Methods: Here, we report a rapid and efficient protocol based on defined culture conditions capable of differentiating adult adipose-derived stem cells (ADSC) to scalable amounts of proliferative melanocyte precursors (PreMel) within 30 days. PreMel were characterized in vitro through qPCR, Western blot, flow cytometry, biochemical assays, and in vivo assays in immunocompromised mice (NOD.Cg-Prkdc^{scid} Il2rg^{tm1Wjl}/SzJ, or NSG).

Results: After 30 days of differentiation, the stem cell-derived PreMel were defined as CD105^{neg} CD73^{low} according to immunophenotypic changes in comparison with parental stem cell markers. In addition, expression of microphthalmia-associated transcription factor (MITF), active tyrosinase (TYR), and the terminal differentiation-involved premelanosome protein (PMEL) were detected. Furthermore, PreMel had the potential to synthesize melanin and package it into melanosomes both in vitro and in vivo in NSG mice skin.

Conclusions: This study proposes a rapid and scalable protocol for the generation of proliferative melanocyte precursors (PreMel) from ADSC. These PreMel display the essential functional characteristics of bona fide HEM, opening a new path for an autologous cellular therapy for vitiligo patients.

Keywords: Melanocytes, ADSC, Vitiligo, Differentiation, MITF, Tyrosinase, Stem cells, CD105

Background

Human epidermal melanocytes (HEM) produce melanin, a pigment responsible for both skin color and protection from ultraviolet radiation (UVR) [1]. Melanin is synthesized in melanosomes and delivered to the surrounding keratinocytes, cells that reside in the epidermis and constitute the defense barrier against UVR [2].

HEM development and differentiation begin with the migration of multipotent progenitors from the neural crest. Expression of transcription factors including paired box gene 3 (PAX3), sex-determining region Y-box 10 (SOX10), lymphoid enhancer-binding factor 1 (LEF1), and microphthalmia-associated transcription factor (MITF) induce the commitment of progenitor cells into melanoblasts and subsequent differentiation into melanocytes when the cells reach the epidermis [3]. There is abundant literature regarding HEM human biology, which is fundamental for the understanding of processes relevant to their development and pathologies such as vitiligo.

* Correspondence: mkhoury@uandes.cl

¹Consortio Regenero, La Plaza 2501, Las Condes, Santiago, Chile

²Laboratory of Nano-Regenerative Medicine, Faculty of Medicine, Universidad de los Andes, Monseñor Álvaro del Portillo 12455, Las Condes, Santiago, Chile

Full list of author information is available at the end of the article



Vitiligo is a pigmentation disease in which the malfunction or apoptosis of HEM generates the disappearance of melanin and, consequently, the generation of white macules in the skin and mucosa [4]. This damage to HEM is generally caused by autoimmune attack, redox unbalance, genetic predisposition, impaired cell adhesion, or dysfunction of the sympathetic nerves, but the consequences to the patient are similar no matter the cause [5]. Vitiligo cases can be classified into two main categories: segmental (SV) and non-segmental (NSV) vitiligo. SV includes cases with rapid stabilization in which the affected areas are not symmetric; these cases are in contrast to those of NSV, which are characterized by a high association with autoimmune disease, symmetric and bilateral macule distribution, and an uncertain disease course [6].

Skin grafts are currently the most promising treatment for stable vitiligo, via application of autologous HEM obtained from healthy zones of the skin directly after biopsy and isolation [7–10]. However, this technique faces one main limitation: the size of the skin biopsy limits the number of isolated epidermal cells and with it the efficiency of the therapy [11–13]. In an approach to transplant HEM expanded in cell culture [14–17], it has been found that HEM from vitiligo patients present low viability and difficulties for *in vitro* management [18–20]. This constraint drives the need to obtain large numbers of HEM or their progenitors without the invasive intervention of large, pigmented skin biopsies. Hence, stem cells represent an attractive source for cell transplantation therapies.

Research addressing this unmet medical need has thus far focused on the development of protocols to encourage HEM differentiation from stem cells. As a therapeutic strategy for vitiligo, the use of pluripotent stem cells including embryonic stem cells (ESC) [21–25], induced pluripotent stem cells (iPS) [26–28], and multilineage-differentiating stress-enduring (MUSE) cells [29, 30] has been explored. Both ESC and iPS displayed high differentiation efficiency but are still limited by safety [31, 32] and ethical issues (for ESC handling). In addition, economic limitations caused by high production costs make these options difficult to justify for a non-fatal disease. Further translational development of these techniques as viable treatment strategies for vitiligo patients has thus been obstructed.

Mesenchymal/stromal stem cells (MSC) have fueled ample research in the regenerative medicine field [33–35] due to their property to differentiate *in vitro* into adipocytes, osteoblasts, chondrocytes, and other cell types [36, 37]. MSC can be isolated from multiple post-natal and adult tissues, which opens the possibility of autologous therapies by allowing cell procurement from any patient. Safe use of MSC in

humans has been demonstrated in several clinical trials [38, 39].

The differentiation of MSC into HEM has been addressed using cells from sources including dental pulp (DP-MSC) [40, 41] and bone marrow (BM-MSC) [42]. However, the differentiation protocols have been shown to be complex and lengthy (reprogramming times of 180–200 days), yielding a low number of HEM; hence, there is no effective protocol currently for the differentiation of adult MSC into HEM. Adipose-derived stem cells (ADSC) have been shown in studies to collaborate with HEM, promoting proliferation *in vitro* and grafting *in vivo* [43, 44].

In this work, we establish a new method for the efficient generation of HEM and their precursors from ADSC. The adipose tissue was selected as the source of choice due to its accessibility, differentiation potential, and clinical safety profile. ADSC differentiation will be guided by a defined culture condition developed by our laboratory in order to obtain a high number of melanocyte precursors or PreMel.

Furthermore, we hypothesize that the improvement of the engraftment can be achieved using proliferative HEM precursors rather than slowly dividing melanocytes. This can also insure a more effective repopulation and re-pigmentation of vitiligo spots.

Methods

All the procedures presented in this work were approved by the Ethics Committee of Universidad de los Andes. All personnel involved in animal studies were trained internally using courses available at www.aalas.org, and assays were performed according to ARRIVE guidelines of the National Centre for the Replacement, Refinement & Reduction of Animals in Research (NC3Rs).

Adipose tissue samples

Adipose tissue (AT) samples were obtained from elective cosmetic liposuction procedures and with the informed consent of donors. All AT donations were from healthy females (18–54 years old) with no reported vitiligo or other autoimmune diseases.

ADSC isolation

ADSC were isolated and cultured as described in Zuk et al. [45]. Lipoaspirates were promptly processed the same day as liposuction under sterile conditions. The AT was transferred to several 50-mL conical tubes and was washed abundantly with phosphate-buffered saline (PBS) pH 7.4 in order to eliminate anesthetics and red blood cells. The AT was digested enzymatically using 0.1% collagenase

type I (Thermo Fisher, MA, USA) for 60 min at 37 °C with gentle agitation. After several steps of centrifugation and washes, a cellular pellet (stromal vascular fraction, SVF) was obtained and was seeded in Dulbecco's modified Eagle's medium (DMEM, Corning, NY, USA) supplemented with 10% fetal bovine serum (FBS, Thermo Fisher), 2 mM L-glutamine, and 100 units/mL penicillin and 100 µg/mL streptomycin (both reagents from Thermo Fisher). The SVF from 50 mL lipoaspirate was seeded in one T175 cm² flask. Non-adherent cells were discarded the next day, while the adherent ADSC were maintained in the previously described culture medium until 80% confluence, when they were harvested using 0.05% trypsin-EDTA (Thermo Fisher) and subcultured. ADSC were maintained in a humidified incubator at 37 °C and 5% CO₂. All experiments were done using cells after four to six subcultures.

The human melanoma cell line A375 (ATCC® CRL-1619™) was kindly gifted from Dr. Manuel Varas (Universidad de los Andes). Fibroblasts were obtained after primary culture of dermal explants. Both cell types were maintained in the same culture conditions as ADSC.

ADSC characterization

ADSC were characterized according to the International Society of Cellular Therapy (ISCT) and International Federation for Adipose Therapeutics and Science (IFATS) guidelines for MSC and ADSC, respectively [46, 47]. Expression of specific markers were evaluated by flow cytometry. Cells were harvested in 0.05% trypsin-EDTA and incubated in cytometry buffer containing specific antibodies (CD90-APC, CD105-PE, CD73-PB, CD44-FITC, CD34-APC, CD45-PECy7, HLA-DR-FITC, CD14-PE, CD31-PE, CD117-APC, CD146-FITC, CD13-APC, and CD106-PE) for 30 min at 4 °C. Samples were analyzed by BD FACS Canto II (BD Biosciences, CA, USA) and FlowJo software V10 (Tree Star, Ashland, OR, USA). Ten thousand events were collected for each sample, and doublets were discarded for analysis purposes.

The same antibody staining procedure was used to characterize PreMel and HEM. Changes between control and differentiated cell populations were determined by comparing the differences in the geometric mean fluorescence intensity (MFI) ratios for each surface marker, calculated as MFI ratio = MFI (specific marker)/MFI (autofluorescence).

For multipotent differentiation, ADSC or PreMel were seeded in 24-well plates at a density of 5×10^4 cells/well and were stimulated with specific inductor media. For osteogenic induction, cells were treated

with DMEM supplemented with 5% FBS, 2.17 mg/mL β-glycerophosphate (Sigma Aldrich, MO, USA), 50 µg/mL ascorbic acid (Sigma Aldrich), and 0.1 µM dexamethasone (Sigma Aldrich). Adipogenic induction was induced with DMEM supplemented with 5% FBS, 0.01 mg/mL insulin (Thermo Fisher), 100 µM indomethacin (Sigma Aldrich), 1 µM dexamethasone (Sigma Aldrich), and 0.25 mM isobutylmethylxanthine (Sigma Aldrich). In both protocols, cells were treated for 14 days. Chondrogenic differentiation was accomplished in 7 days with StemPro® Chondrogenesis Differentiation Kit (Thermo Fisher), according to the manufacturer's guidelines.

Differentiation was determined using specific staining: Alizarin red S, Oil red O, and Safranin O dyes for osteogenic, adipogenic, and chondrogenic lineages, respectively.

ADSC were also characterized by fibroblast colony-forming unit frequency (CFU-F). ADSC were seeded between 0.5 and 50 cells/cm² for 11 days. Later, the cells were fixed with 70% chilled methanol and stained with a 0.05% crystal violet (CV) solution. Colonies of more than 50 cells were counted under a magnifying glass, and CV was dissolved with 1% SDS to measure the absorbance at 540 nm using a spectrophotometer (Tecan Reader).

HEM cell culture

HEM (C1025C, Thermo Fisher) were derived from neonatal foreskin and maintained in M254 medium (Thermo Fisher) supplemented with human melanocyte growth supplement-2 (HGMS-2) PMA-free (Thermo Fisher), which includes 0.2% bovine pituitary extract (BPE), 0.5% FBS, 3 ng/mL human recombinant FGF2, 0.5 µM hydrocortisone, 5 µg/mL insulin, 5 µg/mL transferrin, 3 µg/mL heparin, and 10 nM endothelin-1.

ADSC differentiation into melanocytes lineage

ADSC were seeded at 2×10^3 cells/cm², and the next day, cell culture medium was eliminated and the cells were washed with PBS. Differentiation was induced with an induction medium developed in our lab composed of MCDB 153 (Sigma Aldrich) supplemented with 2% FBS, 2 mM L-glutamine, 100 units/mL penicillin and 100 µg/mL streptomycin, 0.5 µg/mL hydrocortisone (Sigma Aldrich), 50 µM DBcAMP (Sigma Aldrich), 1% insulin-transferrin-selenium (ITS-X) (Thermo Fisher), 4 ng/mL FGF2 (Thermo Fisher), and 20 ng/mL of αMSH (Sigma Aldrich). The growth medium was changed twice a week, and cells were subcultured at 80% confluence. Differentiation conditions were maintained for 30 days, after which cells were characterized.

Quantitative real-time PCR analysis

Total mRNA was extracted from control and PreMel cells at different time points using TRIzol® Reagent (Thermo Fisher), and cDNA was synthesized by reverse transcription. The cDNA samples were analyzed by qPCR to determine the expression levels of different melanocyte markers using *GAPDH* as a normalizing gene (Table 1).

Immunofluorescence detection of MITF, PMEL, and TYR

After 30 days of differentiation, PreMel were seeded in glass coverslips and after 24 h were fixed in 4% paraformaldehyde (PFA) for 15 min at room temperature. The cells were permeabilized and blocked in PBS containing 0.2% Triton X-100 and 1% bovine serum albumin (BSA) for 30 min. The cells were incubated with respective antibodies: mouse anti-human PMEL (HMB45 clone, #cat M0634, DAKO, RRID:AB_2335682), rabbit anti-MITF (cat# 122982, Abcam, RRID:AB_10902226), or mouse anti-tyrosinase (#cat sc20035, Santa Cruz, RRID:AB_628420) at 4 °C overnight. After the incubation, the cells were washed in PBS and stained with the secondary antibodies: goat anti-mouse DyLight® 488 (35502, Thermo Fisher) or goat anti-rabbit DyLight® 594 (35561, Thermo Fisher). 4', 6-Diamidino-2-phenylindole (DAPI, Sigma Aldrich) was used for nuclear staining. Coverslips were mounted in FluorSave™ (Merck Millipore, MO, USA) prior to fluorescence microscopy analysis (ECLIPSE TE2000U, Nikon).

Western blot for MITF and TYR determination

Cell lysates were obtained from control and differentiated cells. At different time points, the cells were washed with cold PBS, lysis buffer was added, and a cell scraper was used for optimized lysis. The lysis buffer contained

70 mM SDS, 50 mM Tris-HCl pH 6.8, and 10% glycerol and was enriched with Protease Inhibitor Cocktail (Sigma Aldrich). Lysates were centrifuged for 10 min at 10,000×g and 4 °C. A Bradford assay (BioRad, CA, USA) was used for protein quantification. SDS-polyacrylamide gel electrophoresis of cell lysates was conducted using a 7.5% acrylamide gel. Thirty to 50 µg cell lysate was loaded into each well with 5 µL protein standard (Precision Plus Protein™ Kaleidoscope™ Prestained Protein Standards, BioRad). Proteins were subsequently transferred to a 0.45-µm pore nitrocellulose membrane.

The membranes were blocked with 5% BSA in 0.1% Tris-buffered saline buffer-Tween 20 (TBST) for 1 h at room temperature. The membranes were incubated overnight at 4 °C in blocking solution with the primary antibodies anti-MITF (1/3000), TYR (1/500), or rabbit anti-vinculin (1/5000, #cat 129002, Abcam, RRID:AB_11144129). After several washes, the membranes were incubated with the secondary antibody goat anti-mouse IgG Alexa Fluor® plus 680 (A32729, 1/15000, Invitrogen), or goat anti-rabbit IgG Alexa Fluor® plus 800 (A32735, 1/25000, Invitrogen) for 1 h at room temperature in the dark. Finally, the membranes were washed four times in PBS and revealed using the Odyssey® CLx Imaging System. For quantification and image analysis, Image Studio™ Lite software was used.

Proliferation assay

1 × 10³ cells were seeded in a 96-well plate in a specific medium (DMEM 10% FBS for ADSC, inductive medium for PreMel, and M254 supplemented with HMGS-2 for HEM). Cell proliferation was estimated through a WST-1 assay (Quick Cell Proliferation Assay Kit, BioVision, CA, USA) according to the manufacturer's guidelines. Briefly, the cells were maintained in 100 µL of their

Table 1 Primers used for qRT-PCR

	Forward	Reverse
MC1R	TTGGACGCTTTCACGCTCTG	TCTGGAACTGAGTGAGCCCT
MITF-M	CAGCGTGTATTTTCCACAG	ATGTCTGGATCATTGACTTGGG
MITF-T	ACTTTAGCTTCTGAGCAAGAGG	CCAAGGAAGTCACAGGCATAAA
PAX3	TCCGAGACAAATACTCAAGGAC	TCACCTTCCCGAATTTACTTCTC
PAX6	CCAGCAACACACCTAGTCATATTC	GCCAGATGTGAAGGAGGAAAC
PMEL	AACTCCAGAGGCTACAGGTATG	GTCTCCACCCACTCTGTAGTT
SOX2	GGAGAGAGAAAGAAAGGGAGAGA	GCCGCCGATGATTGTTATTATTAT
SOX10	ACTTTAGCTTCTGAGCAAGAGG	CCAAGGAAGTCACAGGCATAAA
TRP2	GTACGACAGAGACAAGGAAAGTAAG	CCCAAGCAACTGAGCAGAAA
TYR	GATTGTCTGTAGCCGATTGGAG	GGGTTCTGGATTTGTCATGGT
IL-6	AAATTCGGTACATCTCGACGGCA	AGTGCCTCTTGTCTGCTTTCACAC
TGF-β1	TGGACTTCGGCCACATCAAGAAGA	TGTTGTAAGGGCCAGGACCTGAT
GAPDH	CAGCCTCAAGATCATCAGCA	CATGAGTCTTCCACGATAC

specific medium, and 10 μ L of WST-1 was added per well. The cells were incubated at 37 °C in a cell incubator for 2 h, and the supernatant was transferred into a 96-well flat-bottom plate to measure the absorbance at 450 nm (620 nm reference) in a spectrophotometer (Tecan Reader). The seeded cell culture plate was washed one time with PBS, and fresh medium was added to continue the cell culture. UVR (type B radiation) treatment was done 24 h after cell seeding: cell medium was discarded, and each well was washed with PBS, then 50 μ L PBS was added per well. The 96-well plate was placed under a UVB lamp (UVM57 lamp, UVP Ultra-Violet Products, USA) for 10 or 20 s of illumination (each second is equivalent to approximately 1 mJ/cm²). PBS was then discarded and replaced with fresh medium to continue the cell culture until the end of the experiment. Oxidative stress was induced with H₂O₂ (Merck Millipore) at different concentrations in the cell-specific media, and the cells were stimulated at the fourth day after seeding with 0, 50, 100, 300, and 500 μ M H₂O₂ for 24 h. After the stimulus, the medium was eliminated, cells were washed, and fresh medium was added. The supernatants were recovered for spectrophotometer measurements. For each experiment, the cells were maintained in cell culture conditions until the end of the assay. Population doubling time (PDT) and growth rate (GR) were determined with the Exponential Growth Curve tool from GraphPad Prism version 5.0b for Windows (La Jolla, CA, USA).

L-DOPA (3, 4-dihydroxyphenylalanine) assay

TYR enzymatic activity was determined through the L-DOPA assay. Qualitative cell staining and quantitative L-DOPA oxidation measurements were performed. Cells were seeded at 5 \times 10³ cells/cm² for L-DOPA assay staining; next day, the medium was discarded, and the cells were fixed in 4% PFA. Cells were then incubated with fresh 0.1% L-DOPA in PBS (pH 6.8) at 37 °C for 2 h. The samples were washed in PBS and photographed with the Olympus CX41 microscope. For L-DOPA determination in cell lysates, cells were washed with PBS and lysed with a minimum volume of lysis buffer (1% Triton X-100 in PBS pH 6.8). Cells were frozen at -80 °C for at least 20 min and were thawed for 10 min at room temperature in gentle agitation, lysed mechanically with a pipette tip, and centrifuged at 13,000 \times g for 15 min at 4 °C. The supernatants were collected, and absorbance was measured at 595 nm for protein quantification via the Bradford method. 0.1% L-DOPA was prepared fresh in PBS pH 6.8, and 10 μ L of this substrate was added to 25 μ g proteins suspended in 90 μ L total volume. Samples were incubated at 37 °C, and absorbance was measured at 475 nm each 30 min for 10 h. All

measurements were made in a NanoQuant Infinite TECAN M200 PRO.

Melanin determination

For cellular melanin determination [48], cells were washed in PBS, trypsinized, and counted. The cells were lysed in 1 M NaOH with 10% DMSO at 80 °C for 1 h. After centrifugation at 10,000 \times g for 5 min, absorbance was measured at 415 nm using a standard curve of synthetic melanin (Sigma Aldrich). All measurements were normalized according to cell number or protein concentration.

Transmission electron microscopy

Localization and stage of melanosome development were determined by TEM as described by Paino et al. [40]. Cells were fixed in 2.5% glutaraldehyde in 0.1 M cacodylate buffer and post-fixed in 1% OsO₄. After dehydration, the samples were mounted for analysis with SEM LEO 1420VP transmission electron microscope (Laboratorio de Microscopía Electrónica de Barrido SEM, Pontificia Universidad Católica de Chile).

PreMel transplantation

To evaluate PreMel grafting and melanin synthesis in vivo, cells were injected into the dorsal skin of 8-week-old immunocompromised male mice (NOD.Cg-Prkdc^{scid} Il2rg^{tm1Wjl}/SzJ) or NSG) according to the methods described by Alexeev and Yoon [49]. Mice were anesthetized with 3–5% sevoflurane inhalation, and hair removal was performed using an electric shaver and a hair removal cream for 2 min. 1 \times 10⁶ cells (PreMel, HEM or ADSC) were suspended in 50 μ L saline and were applied to the mice intradermally using a tuberculin syringe, with three injections per animal. Animals were maintained under standard conditions (water and food ad libitum) and after 2 weeks were euthanized with CO₂ inhalation for skin analysis.

Melanin determination in mouse skin

Melanin determination was made according to the methods of Yamamoto et al. [50] with modifications. After euthanasia, the portion of the skin that was injected with cells was extracted, weighed, and boiled in 10 mL 0.1 M acetic acid for 10 min. When the suspension was cooled, absorbance was measured at 415 nm. The following steps from the original protocol were not completed due to the vascularization of the back of the skin, which could have generated excessive noise in the absorbance measurements following complete digestion of the tissue, especially when the expected results were discrete.

Immunohistochemistry of PreMel grafted in mouse skin

After the *in vivo* assay, the mouse skin was removed and fixed in 10% formalin solution (Sigma Aldrich) for 16 h at room temperature. After several washes with PBS, the tissue was dehydrated using a battery of ascending concentrations of alcohols and xylene, after which tissues were embedded in paraffin. Samples were cut into 5- μ m sections in a microtome. For immunohistochemistry, slides were stained with the antibody anti TYR (permeabilization needed) or CD90-FITC. DAPI was used for nuclear staining, and samples were mounted with Fluorsave. Subsequently, slides were analyzed with the Sp8 confocal microscope (Leica) and LAS X software (V 3.3.0.16799).

Fontana-Masson staining

Melanin determination in mouse skin after PreMel grafting was done using the Fontana-Masson staining kit according to the manufacturer's instructions (Abcam). Briefly, samples were incubated with 10% pre-warmed silver nitrate solution at 60 °C for 60 min. After washes and posterior treatment, the samples were counterstained with Nuclear Fast Red for nuclear visualization. Pictures were taken with the Olympus CX41 microscope.

Statistics

All assays were performed at least in triplicate using three to five different human donor samples. Values are shown as mean \pm SEM, and statistical significance was estimated using Student's unpaired *t* test or analysis of variance (ANOVA), $P < 0.05$ was considered as statistically significant. The software GraphPad Prism 5.0b was used for statistical analysis.

Results

PreMel display a combined immunophenotype of ADSC and HEM surface markers

ADSC are isolated from the heterogeneous SVF of adipose tissue and need to be characterized according to the guidelines from the ISCT and IFATS to be considered MSC [46, 47]. First, we analyzed the expression of several classic mesenchymal markers. ADSC were positive for CD105, CD90, CD73, and CD13 in more than 95% of the cell population; CD44 was also positive in a minority of the population (Additional file 1: Figure S1A-E). Likewise, ADSC are negative for CD31, CD14, CD45, and CD106 and partially positive for CD34 (Additional file 1: Figure S1F-J). Additionally, ADSC have the potential to differentiate into adipogenic, chondrogenic, and osteogenic tissue *in vitro* in response to specific inductive media as was shown by positive lineage-specific

stainings: Red Oil O, Safranin O, and Alizarin Red S, respectively (Additional file 1: Figure S1K-M). The capacity for ADSC self-renewal was estimated using a CFU-F assay showing the progenitor frequency (Additional file 1: Figure S1N). All these properties taken together confirm the MSC signature of ADSC.

As ADSC present a differentiation potential *in vitro*, we developed a defined medium to induce the differentiation of ADSC into HEM and evaluated the changes in the expression of the abovementioned markers by flow cytometry (details of the gating strategy are displayed in Additional file 2: Figure S2).

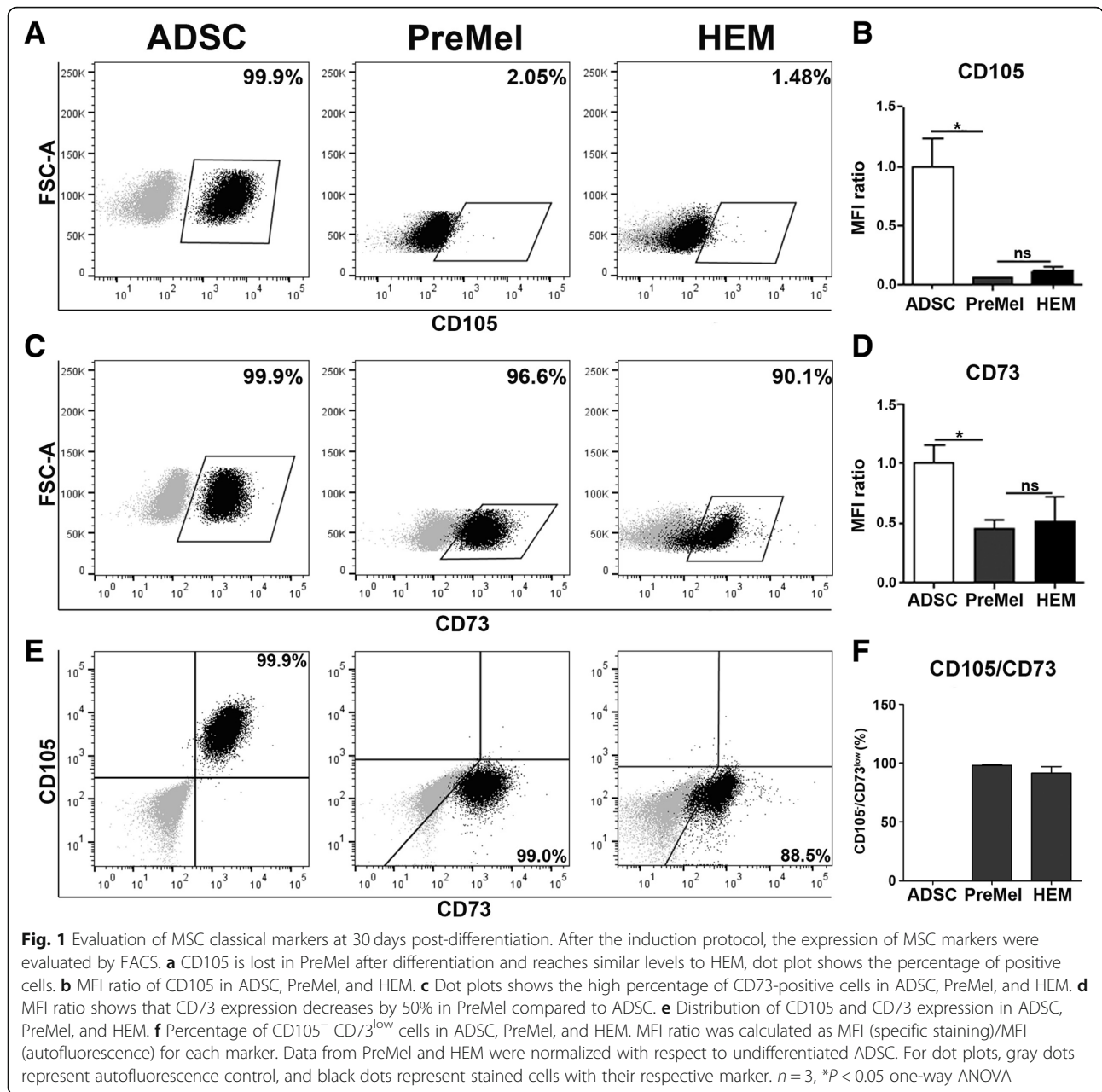
CD105 was highly expressed in ADSC ($99.8\% \pm 0.12\%$ positive cells), but it was absent in PreMel ($0.36\% \pm 0.25\%$ positive cells). Notably, HEM also expressed very low and variable levels ($11.9\% \pm 7.83\%$) of CD105 (Fig. 1a, Table 2). The MFI ratio also showed that the level of expression of CD105 diminished significantly in PreMel with respect to ADSC and was very similar to HEM (Fig. 1b).

Furthermore, a 50% decrease in the MFI ratio was also observed for the expression of CD73 in PreMel with respect to ADSC, albeit the entire population remained positive ($98.2\% \pm 1.46\%$) (Fig. 1c, Table 2). Both MFI ratio and percentages were comparable with HEM expression, reaching a similar level ($91.4\% \pm 9.87\%$) (Fig. 1c, d).

Other markers, such as CD44 and CD146, that were positive in ADSC remained unchanged following the differentiation protocol (Additional file 3: Figure S3A-B, 3E-F, respectively). A slight decrease was detected for CD90 expression in PreMel, but it was not statistically significant (Additional file 3: Figure S3C-D). CD117 expression increased in PreMel, but the percentage of positive cells was too low to be considered significant (Additional file 3: Figure S3G-H). CD45, CD31, CD14, and HLA-DR were not detected in ADSC, PreMel, or HEM (data not shown).

An important change of CD105 and CD73 expression was detected following the differentiation protocol (Fig. 1e, f; Table 2). The co-expression of these two markers in PreMel was notably similar to that in HEM ($98.2\% \pm 1.46\%$ vs $91.4\% \pm 9.87\%$, respectively) but differs significantly from that in ADSC ($0.11\% \pm 0.20\%$). Hence, PreMel cells were designated as the CD105^{neg} CD73^{low} cell population.

Since adipogenic differentiation of ADSC is another gold standard property of MSC (Additional file 1: Figure S1M), we evaluated whether PreMel retained this potential following the 4-week induction protocol. Interestingly, PreMel displayed a significantly lower number of Oil Red O⁺ cells in comparison with ADSC (Additional file 4: Figure S4). The decrease in the adipogenic differentiation potential of PreMel along with the diminished expression of CD105-



CD73 with respect to ADSC are indicators of the loss of their MSC identity and suggest a change of their cell fate.

Rapid and efficient differentiation of ADSC into PreMel

We then evaluated whether the loss of the MSC signature in PreMel was compensated with a gain in

HEM features. ADSC were stimulated for 4 weeks, and cell morphology and gene expression were evaluated. The shape of ADSC in cell culture was generally fibroblastoid (Fig. 2a). After the first week, a change in cell morphology was observed where the fibroblastoid shape became more elongated and

Table 2 Expression of CD105 and CD73 in ADSC, PreMel, and HEM (percentage of positive cells ± SD)

	CD105 ⁺ CD73 ⁺	CD105 ⁺	CD73 ^{+/low}	CD105 ^{neg} CD73 ^{low}	CD105 ^{neg} CD73 ^{neg}
ADSC	99.2 ± 0.53	99.8 ± 0.12	99.4 ± 0.52	0.11 ± 0.20	0.12 ± 0.2
PreMel	0.29 ± 0.21	0.36 ± 0.25	98.2 ± 1.46	98.2 ± 1.46	1.78 ± 1.44
HEM	11.4 ± 8.23	11.9 ± 7.83	91.4 ± 9.87	91.4 ± 9.87	7.65 ± 9.67

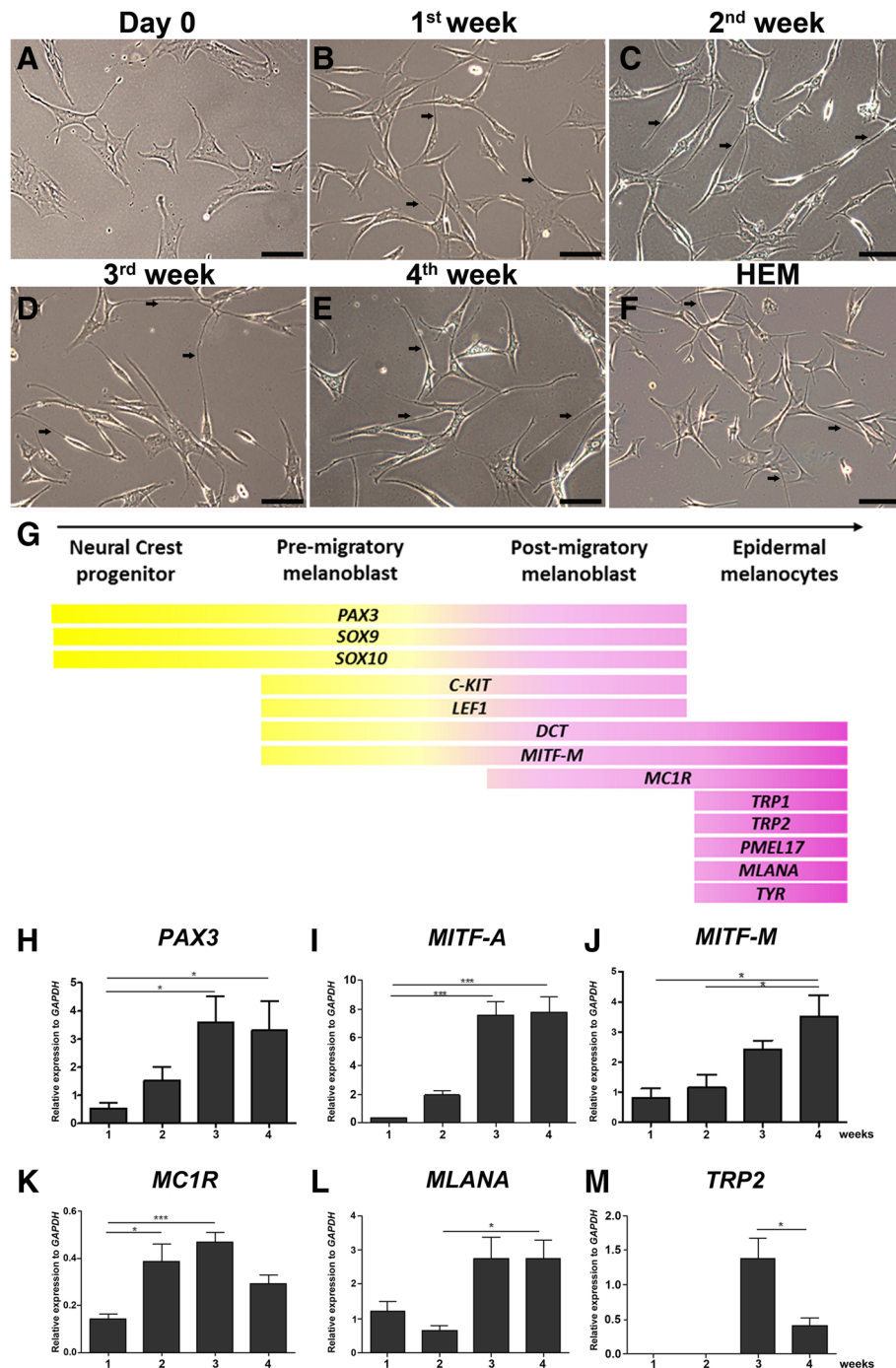


Fig. 2 PreMel and HEM share a common gene transcription pattern. **a** Phase-contrast images show ADSC fibroblastoid morphology in control conditions. **b** After 1 week of differentiation, long and thin cellular extensions are observed. **c** Along with these cellular protrusions, the entire cells look thinner with respect to **a**. This phenotype continues after the third (**d**) and fourth (**e**) week and resembles the phenotype of HEM (**f**). Black arrows highlight the long cellular protrusions. Scale bar = 250 μ m. **g** Scheme of different stages and gene expression of HEM during mammalian differentiation. Some of these genes were evaluated during ADSC differentiation protocol. **h** *PAX3* shows a constant increment during the protocol with a significant increase after 3 and 4 weeks. The same pattern is seen with **i** *MITF-A* and **j** *MITF-M*. **k** *MC1R* transcript increases significantly from the second week. **l** *MLANA* appears mostly during the second part of the protocol. **m** *TRP2* expression is detected after 3 weeks of differentiation. $n = 3$, $*P < 0.05$ one-way ANOVA; statistical analysis was calculated with respect to the first week of differentiation. Non-differentiated ADSC were used as a control

displayed bipolar forms (Fig. 2b). After 2 weeks, the cells acquired a bipolar shape with long processes (Fig. 2c). The observed phenotype was even pronounced after 3–4 weeks (Fig. 2d, e), and cell morphology was highly heterogeneous between ADSC-like cells and melanocyte-like cells (Fig. 2f).

Molecular signature of PreMel

During the differentiation of HEM, each stage is characterized by the expression of specific genes (Fig. 2g). To evaluate the differentiation of ADSC into PreMel, we analyzed a panel of genes during the induction protocol: *PAX3*, *MITF-A*, *MITF-M*, melanocortin receptor 1 (*MC1R*), protein melan-A (*MLANA*), and tyrosinase-related protein 2 (*TRP2*). Other genes were also evaluated, but transcripts barely reached detection level in PreMel (data not shown).

The differentiation protocol induced a continuous increase of *PAX3*, *MITF-A*, and *MITF-M* reaching a maximum during the third to fourth week (Fig. 2h–j). Additionally, we analyzed the levels of *MC1R*, *MLANA*, and *TRP2* which represent later stages of HEM development. *MC1R* increased since the beginning of the differentiation protocol, reaching a maximum in the third week (Fig. 2k). Also, there was an increment for both *MLANA* and *TRP2* since the third week (Fig. 2l, m).

In addition, a more complete panel of genes was evaluated in HEM and A375, an amelanotic melanoma cell line, as positives control (Additional file 5: Figure S5).

PreMel express the melanocyte-specific proteins: MITF, TYR, and PMEL

To determine the commitment level of the PreMel population within the melanocyte lineage stages, we analyzed the expression of melanocyte-specific proteins: MITF as a marker for the entire lineage (progenitors and HEM), and TYR and PMEL for terminal differentiation.

While MITF expression was detected in the entire cell population of PreMel and HEM by immunofluorescence and FACS (Additional file 6: Figure S6), we were unable to determine whether the protein corresponded to the isoform A or M; hence, we analyzed the MITF expression by Western blot.

In HEM lysates, we detected two isoforms of MITF according to their molecular weight (MW): one band at 75 kDa and two bands with a MW close to 70 kDa. The 75-kDa band corresponds to the MITF-A isoform, and the doublet corresponds to MITF-M (specifically expressed in HEM) in different phosphorylation states (Fig. 3a). In the cell line A375, both isoforms were detected. MITF-A and MITF-M were almost absent in ADSC but appeared during the first week of induction in PreMel, with a constant increase until the fourth week as shown in the quantification plot (Fig. 3a–c). These

results evidence the inductive effect of the differentiation protocol through the activation of the signaling pathways that command the transcription and translation of the MITF gene, and we were able to detect both A and M isoforms in PreMel.

Immunofluorescence analysis showed the distribution of MITF; in HEM and PreMel, there was a strong nuclear stain, but the protein was also visualized in the cytoplasm. In ADSC, we observed the protein both in the cytoplasm and the nucleus but in a minority of cells (Fig. 3f–h).

Analyzing the expression of MITF by immunofluorescence and Western blot results altogether pointed at the expression of MITF-A and MITF-M by both HEM and PreMel (Fig. 3a, f, g). However, the cellular distribution of the specific isoforms was not determined, which can be relevant to suggest the transcriptional activity of MITF-M in PreMel. For this, we measured the fluorescence intensity of MITF in the cytoplasm and nuclei of HEM, ADSC, and PreMel in order to determine if the distribution of the transcription factor in PreMel was similar to HEM or ADSC. DAPI was used as an absolute nuclear staining control. In HEM, MITF was distributed both in the nucleus and the cytoplasm, with higher enrichment in the latter. A similar distribution was detected in PreMel, and a more pronounced cytoplasmic distribution was detected in ADSC (Fig. 3i). This result showed that the differentiation process induced an accumulation and redistribution of MITF in the nuclei of PreMel similar to its distribution in HEM, as both isoforms were expressed in PreMel (according to the Western blot). Therefore, MITF-A can be accumulated as much as MITF-M in the nucleus in an unknown proportion.

TYR and PMEL are HEM-specific proteins and transcriptional targets of MITF-M [51, 52]. Therefore, we analyzed their expression in ADSC, PreMel, and HEM cells. TYR expression analysis in HEM showed a band of 80 kDa that corresponds to the *N*-glycosylated isoform and several smaller bands corresponding to lesser *N*-glycosylated forms of the enzyme [53]. In A375 cells, TYR was also detected but only in its main isoform (Fig. 3a). TYR was absent in ADSC, but after 2 weeks of differentiation, the protein was expressed in PreMel as a result of the induction protocol (Fig. 3a–e). Immunofluorescence of TYR showed a cytoplasmic localization in $12.12\% \pm 5.2\%$ of the cells (Fig. 3j–m). PMEL also had a cytoplasmic localization as expected, and positive cells were quantified as $10.62\% \pm 4.3\%$ (Fig. 3n–q). These results showed that the PreMel not only express MITF-A and MITF-M, but also TYR, the main component of the melanin enzymatic machinery, and PMEL, a structural component of melanosomes, to a lesser degree. In summary, 100% of PreMel were MITF⁺ (A or M), around

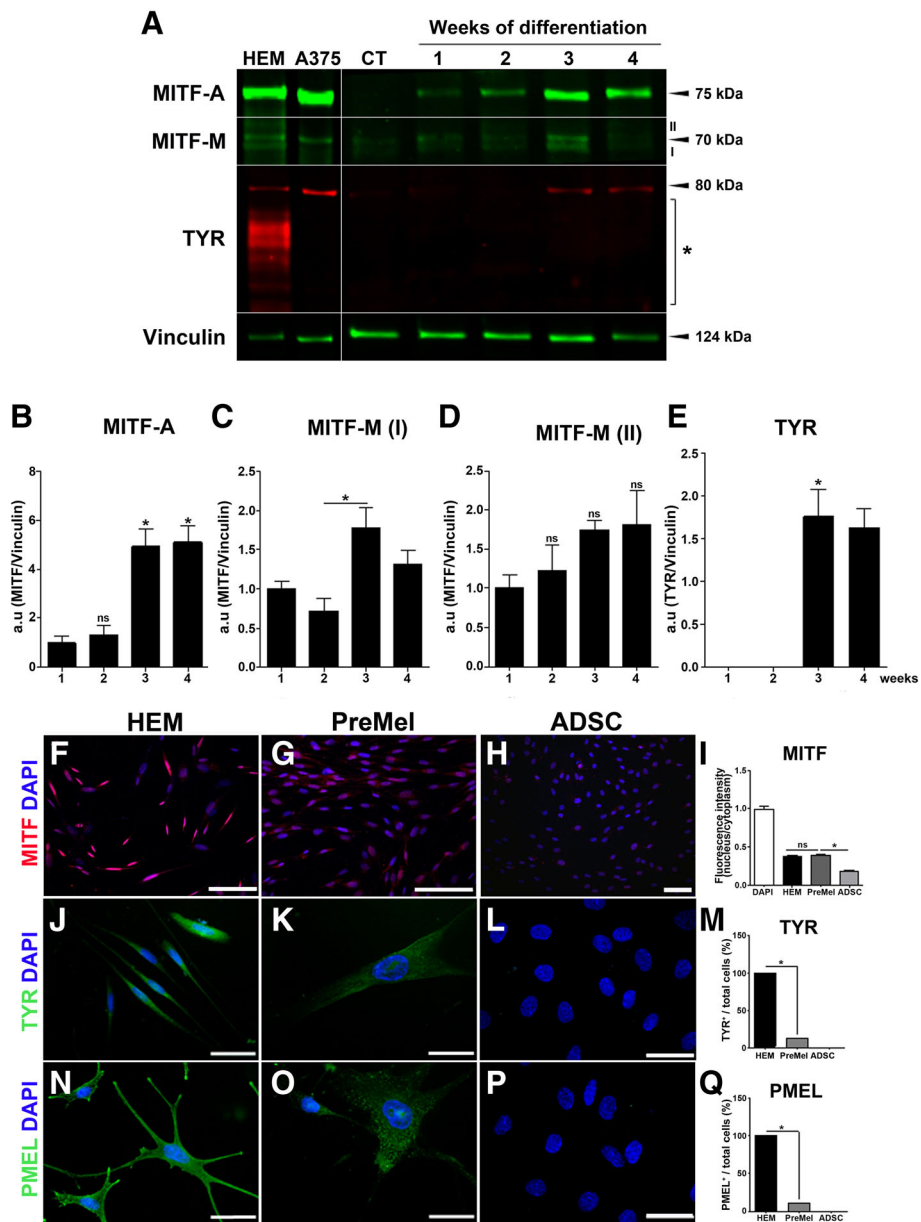


Fig. 3 PreMel express HEM-specific proteins. Expression of MITF and TYR was evaluated by Western blot in HEM, A375 cells, ADSC, and PreMel. **a** In HEM and A375 cells, there is a band at 75 kDa and a doublet at 70 kDa, which represent MITF-A and MITF-M isoforms, respectively. Bands were denominated as I (lower band) or II (upper band) only for quantification. The reported band for *N*-glycosylated TYR is 80 kDa, but in HEM, multiple bands (*) appear that correspond to less *N*-glycosylated forms of the enzyme. Vinculin was used as a loading control. **b** Quantification shows that there is a significant increase in MITF-A levels in PreMel. **c-d** Each band of the MITF-M doublet was quantified as I and II. **e** TYR protein levels rise in response to the differentiation induction. **f** MITF localization in HEM is both nuclear and cytoplasmic. **g** MITF distributes similarly in PreMel compare to HEM. **h** ADSC express lower levels of MITF. **i** Nucleus/cytoplasm ratio of fluorescence intensity of MITF shows that the cellular distribution of MITF is similar between PreMel and HEM. Data are normalized with respect to DAPI intensity. TYR localization is cytoplasmic in **j** HEM and **k** PreMel, but not all differentiated cells are positive for TYR. **l** In ADSC, TYR is not detectable. **m** Quantification of TYR⁺ HEM, ADSC, and PreMel. A similar pattern is observed for PMEL in **n** HEM and **o** PreMel, with a low percentage of positive cells. **p** There is no expression of PMEL in ADSC. **q** Quantification of PMEL⁺ HEM, ADSC and PreMel. Scale bar = 100 μ m (**f-g**) and 50 μ m (**j-p**). *n* = 3, **P* < 0.05 one-way ANOVA, compared to ADSC

12% of PreMel were TYR⁺, and 10% of cells were PMEL⁺. Hence, PreMel can be characterized as a mixed population of MITF⁺ cells with subpopulations of TYR⁺ and PMEL⁺ cells.

Similarities between PreMel and HEM cell cycles

We evaluate the cell cycle of PreMel in vitro as compared with ADSC and HEM. At the end of the exponential phase (day 6), the cell number of ADSC was 2.2× higher than PreMel and HEM, while no difference was detected among those two types. At the end of the growth curve, ADSC reached a cell number 4.3× higher than PreMel and HEM, but the similarities between these two types remained (Additional file 7: Figure S7A). Population doubling time (PDT) and the growth rate (GR) were calculated to demonstrate the similarities between the cell cycles of PreMel and HEM (Additional file 7: Figure S7B).

Likewise, as HEM are exposed daily to physiological injuries, such as UVR and the presence of reactive oxygen species (ROS), we simulated and evaluated the effect of these two parameters over the cell cycle. At 10 or 20 mJ/cm² UVR, both PreMel and HEM were slightly and similarly affected by the radiation without significant changes to either PDT or GR (Additional file 7: Figure S7B). Additionally, we evaluated the effect of oxidative stress over cell proliferation. While all the cells analyzed were affected by the presence of H₂O₂, ADSC and PreMel showed similar sensibility to the tested concentrations (Additional file 7: Figure S7C).

Measurement of TYR activity in PreMel

TYR is essential for the synthesis of melanin; hence, we evaluated their activity with the L-DOPA assay in PreMel. First, we evaluated the generation of a dark deposit in cell cultures through phase-contrast microscopy. ADSC were negative for dark granules (Fig. 4a), and PreMel showed a slight dark coloration compared with the PBS control (Fig. 4b), but brighter in comparison with the strong dark color in HEM (Fig. 4c). No deposits were distinguished in either A375 cells or fibroblast samples (Fig. 4d, e). As L-DOPA assay visualization by phase-contrast microscopy is unable to detect low levels of TYR activity, we performed a L-DOPA assay in which the oxidation of the substrate was measured by absorbance over time. After 6 h of incubation, there was a significant difference in the absorbance in PreMel showing the oxidative activity of TYR over the background noise that was obtained in ADSC. This result evidences that PreMel express TYR (Fig. 3) in its active form. Between 4 and 6 h post-incubation, a peak in TYR activity was observed in PreMel although it remained below HEM activity in accordance with immunofluorescence data showing that 12% of PreMel were TYR⁺ and that the

enzymatic activity detected must come from these specific cells. In fibroblasts and A375 samples, there was a slight increase in absorbance, but this was likely due to the background noise or the L-DOPA oxidation expected over time. No statistical differences were obtained between the two cell types, confirming the assay specificity.

Evidence of melanin synthesis and melanosome biogenesis

Melanin is the end product of a series of enzymatic reactions that take place inside the melanosome. Consequently, we evaluated if PreMel were capable of synthesizing melanin in vitro and packaging it into melanosomes. First, we observed that the color of the cellular pellet of PreMel was darker than ADSC (Fig. 5a) and lighter than HEM, and this was correlated with the mean gray value of the pellets (Fig. 5b). Next, we determined the presence of melanin in PreMel lysates using synthetic melanin as a standard, and we showed an absorbance significantly higher than ADSC (unspecific absorbance at the respective wavelength) but lower than HEM. This again confirmed that PreMel are functionally closer to HEM and possess the capacity to synthesize melanin. (Fig. 5c). Remarkably, two cytokines related with whitening effects of ADSC in the skin through TYR inhibition activity, *TGF-β1* and *IL-6*, were downregulated after the 4-week differentiation protocol in PreMel (Additional file 8: Figure S8).

Conversely, we analyzed the ultrastructure of PreMel by transmission electronic microscopy (TEM) and identified melanosomes as single-membrane vesicles with dark pigment inside (Fig. 5d–f), similar to the structures present within the HEM cytoplasm (Fig. 5g–i). Such structures were not observed in ADSC (data not shown). We were able to detect melanosomes in PreMel; however, the number of melanosomes in PreMel was considerably lower than in HEM. In HEM, the four stages of melanosome biogenesis (I–IV) were identified, but in PreMel, only stages III and IV were distinguished. Earlier stages could be mistakenly confused with other intracellular formations such as secretory vesicles. Both results support the hypothesis that PreMel represent a population of melanocyte-like cells with melanin synthesis capabilities in vitro.

Engraftment of PreMel in mouse skin and synthesis of melanin in vivo

PreMel were injected in the back skin of immunodeficient mice in order to visualize their HEM-like properties in vivo (Fig. 6a), for this experimental setup, we used albino NSG animals because they lack functional epidermal melanocytes [54]. After 2 weeks, the skin was recovered for histological analysis. First, we quantify the

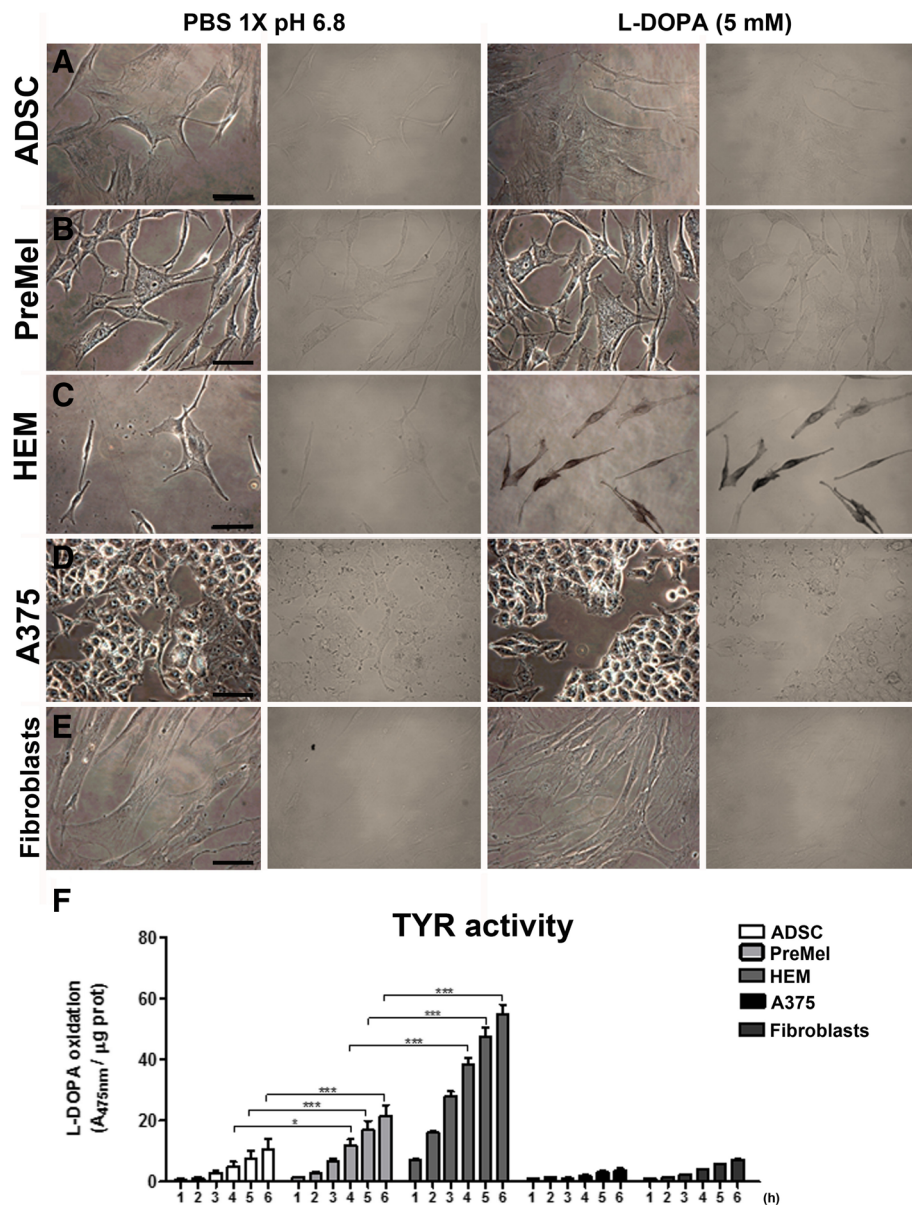
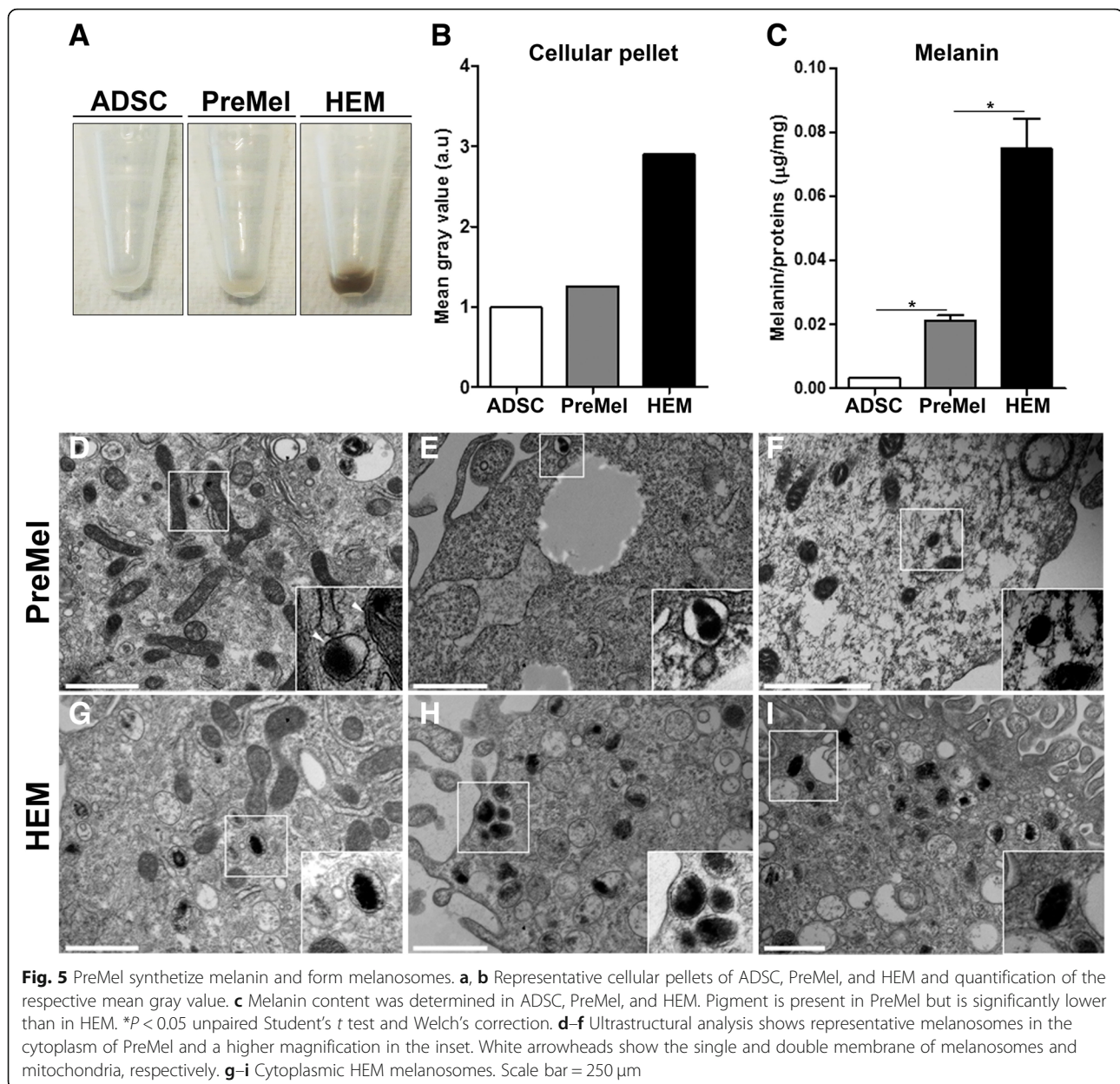


Fig. 4 Measurement of TYR activity of PreMel. L-DOPA assay was performed in cell monolayers of **a** ADSC, **b** PreMel, **c** HEM, **d** A375 cells, and **e** fibroblasts. Second and fourth columns show a different microscope filter to enhance the contrast for dark granule visualization. **f** TYR activity was measured by absorbance in the same cell lines at different time points. L-DOPA oxidation was compared in each time point for statistical analysis. * $P < 0.05$, two-way ANOVA and Bonferroni post-test. ADSC, PreMel, and HEM were compared. Scale bar = 100 μm

presence of melanin in the skin, and we were able to determine that in fact, PreMel synthesize melanin in vivo, but to a lesser extent with respect to HEM (Fig. 6b), possibly because a minor proportion of PreMel has the potential of synthesize and package the melanin (MITF⁺ TYR⁺ PMEL⁺ cells). In order to discard any unspecific measurement, we analyzed microscopically the presence of PreMel. For this, skin slides were stained with the Fontana-Masson stain using human skin as a positive control, where HEM in the basal membrane of the dermis were stained brownish-dark (Fig. 6c). While no

stained cells were detected in the animals injected with ADSC (Fig. 6d), we were able to distinguish positive stained cells in the PreMel-treated animals which demonstrated that injected cells were in fact cells with HEM-like properties (Fig. 6e), reflecting that PreMel behave as HEM in vivo (Fig. 6f). Next, we determined the expression of TYR in PreMel in vivo in the mouse skin, using human skin (Fig. 6g) and injected HEM (Fig. 6f) as positive controls. Notably, we detected TYR⁺ cells in the skin of the animal, cells that were identified as injected PreMel (Fig. 6h), because TYR was not detected



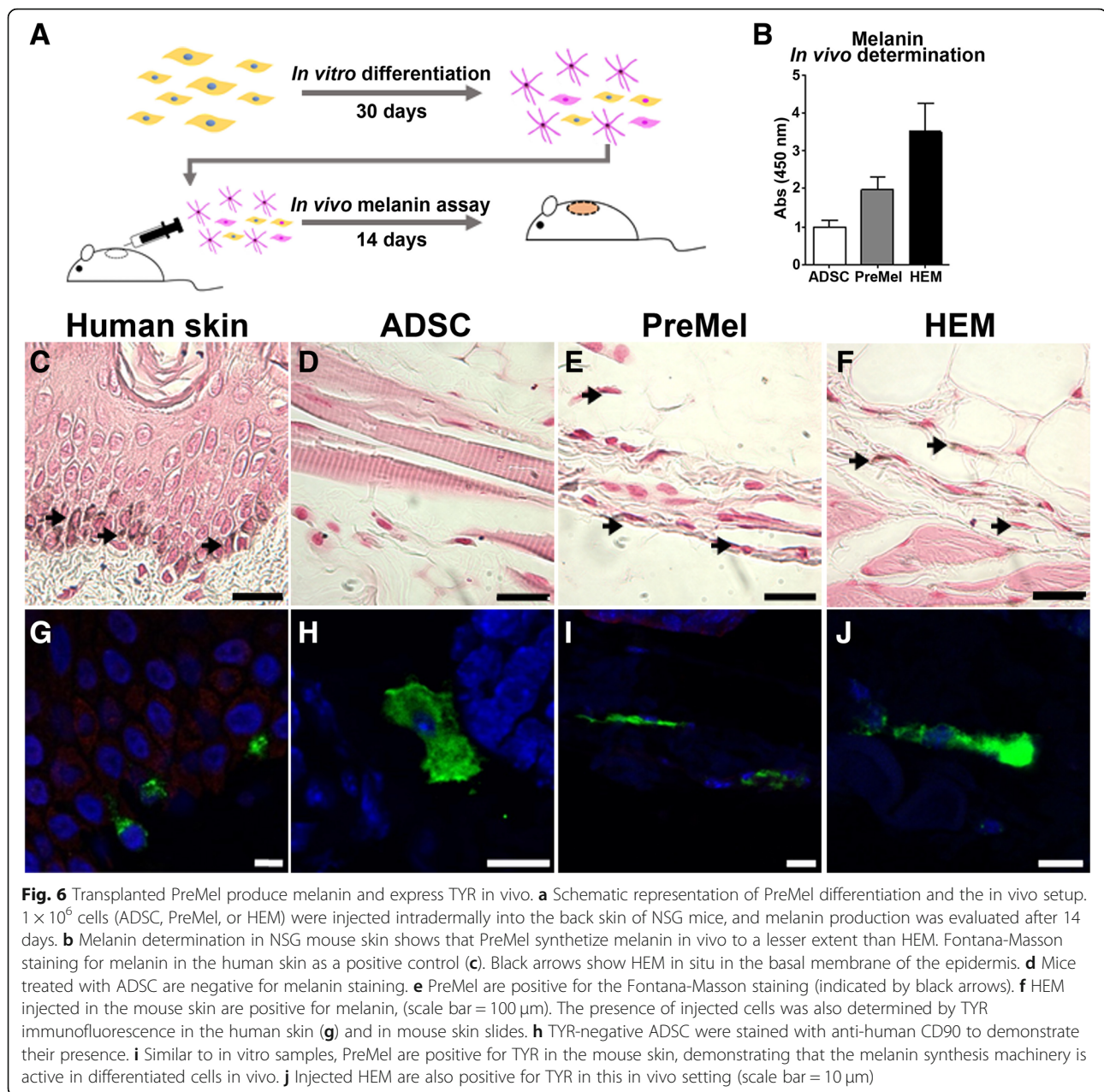
in NSG skin control (data not shown). In animals injected with ADSC, TYR was not detected; however, CD90 was used in order to confirm the presence of the injected human cells (Fig. 6h).

Discussion

To date, the current approach for cell-based therapy for vitiligo is to obtain a large number of HEM in order to replace the lost cells. Although this invasive strategy has shown relative success, multiple biopsies and repetitive treatments are required to obtain the necessary number of cells to complete the entire treatment [11, 12]. Hence, the generation of HEM or their precursors that can

reach function completely in situ is an attractive strategy worth exploring.

Mimicking the conditions of the HEM microenvironment at the molecular level is key for a successful differentiation in vitro. We developed an inductive medium which includes ligands for some of the fundamental pathways involved in HEM differentiation. FGF2 is secreted by keratinocytes [55] and is a potent mitogen for HEM in conjunction with DBcAMP [56], as well as a fundamental role player in HEM differentiation through the activation of *PAX3* transcription through ERK1-dependent STAT3 phosphorylation [55]. DBcAMP penetrates the plasma membrane more easily than cAMP [57] and acts as a potent mitogen and can induce



melanoblasts differentiation into HEM in vitro [56, 58]. α MSH, also secreted by keratinocytes, signals through MC1R and induces an increase in the cAMP levels which activates PKA. Through PKA activation, several MC1R-dependent functions are translated in HEM, including melanin synthesis. Hydrocortisone promotes cell differentiation in HEM cultures [59, 60], and dexamethasone, a synthetic form of it, has been used for ESC differentiation into HEM along with FGF2 and an enhancer of cAMP levels such as DbcAMP [21]. Insulin, transferrin, and selenium have been reported as the supplemental factors for low-serum media [30] but has been shown that insulin in combination with

FGF2 promotes HEM proliferation [61]. The final formulation for our inductive medium was able to effectively recapitulate the HEM developmental stages at a shorter time scale, and consequently, rapid differentiation of ADSC into PreMel was achieved within only 30 days. Ligands from other signaling pathways, such as WNT and endothelin [62, 63] can be added to this protocol in order to increase the proportion of terminally differentiated HEM or to use the co-culture with keratinocytes and/or fibroblasts, which could represent the in vivo niche in an in vitro setting promoting the development and differentiation of PreMel.

The mechanism of differentiation of PreMel in response to the inductive media was explained through the analysis of specific genes expressed in HEM. *PAX3*, a member of the PAX family, is the first transcription factor that was upregulated in PreMel and is also one of the described factors responsible for the commitment of melanoblasts from a neural crest cell, along with others including *SOX9*, *SOX10*, *FOXD3*, *SNAI2*, and *MITF* [64, 65]. *PAX3* recognizes specific domains of the *MITF* promotor [66] and is in part responsible for *MITF* transcription. An increase in *PAX3* expression in PreMel was accompanied with an increase in *MITF* levels starting during the second week of induction. This could also be a result of the presence of other transcription factors described for this role in HEM, such as *SOX10*, *LEF1* (activated by *WNT*/ β -catenin signaling), and *CREB*, not analyzed in this work. Remarkably, *MITF-A* levels were higher than *MITF-M* levels, which could be explained for the differential accessibility to the alternative promoters that are present in the *MITF* gene, being the most proximal to the transcriptional start site (TSS) the one for *MITF-M*, the shortest isoform of the gene [51, 67]. This result suggests that the increase in *MITF* protein levels is mostly represented by the A isoform and that the expression of HEM-specific genes are commanded by *MITF-M*, despite its lower expression levels.

An increase in *MLANA* and *TRP2* during the third week was observed along with the increases in *PAX3* and *MITF-M*, which suggests that the transcriptional activity of the induced levels of *MITF-M* in PreMel are responsible for *MLANA* and *TRP2* expression, as it has been described that *PAX3* cooperates with *MITF-M* in transcription of *TRP2* [68].

On the other hand, *MC1R*, the main regulator of melanin synthesis in HEM [69], was expressed at low levels in ADSC but was upregulated starting in the second week. It is possible that *MC1R* activation is independent of *MITF* and is instead the outcome of a positive feedback loop linked to the presence of *DBcAMP* and α *MSH* in the induction culture media [70]. *MC1R* displayed a two- to threefold increase in the transcript levels in PreMel, compared to ADSC. The expression level remained low (from 0.18 to 0.44) in agreement with the relatively low number of *MC1R* molecules expressed at the HEM surface [71]. Notably, *MC1R* is a GPCR (G protein-coupled receptor) and can undergo desensitization and internalization via the endocytic pathway [70], meaning that the continued presence of α *MSH* during the differentiation protocol does not ensure continuous signaling by *MC1R*.

In addition to the molecular data, the expression of *MITF*, *TYR*, and *PMEL* allow us to estimate a

differentiation yield in PreMel: 100% of PreMel were *MITF*⁺ (A or M), around 12% of PreMel were *TYR*⁺, and 10% of cells were *PMEL*⁺. This suggests that the entire PreMel population could be committed to the HEM lineage (*MITF*⁺ *TYR*⁻ *PMEL*⁻), while only a subpopulation is terminally differentiated as HEM (*MITF*⁺ *TYR*⁺ *PMEL*⁺) and possess melanin synthesis capabilities.

Another relevant parameter evaluated to evidence cell differentiation was the expression of classic MSC markers. According to Dominici et al. [46], *CD105* is listed within the stem cell-associated markers necessary to appropriately identify MSC. While ADSC showed high *CD105* expression, following the differentiation induction protocol, the expression diminished almost completely in PreMel. *CD105*, or endoglin, is a type I transmembrane glycoprotein and is part of the *TGF- β* receptor complex which controls several cellular functions in HEM, including melanin synthesis. *TGF- β 1* inhibits melanin formation through multiple mechanisms [72]: in immortalized melanocytes (Mel-Ab cells), *TGF- β 1* treatment diminishes *TYR* activity, and consequently, melanin synthesis decreases; *TGF- β 1* signaling not only reduces the *MITF* activity promotor, but also decreases the levels of *MITF*, *TYR*, *TRP1*, and *TRP2* proteins [73, 74]. Therefore, diminished *CD105* expression in PreMel after the induction protocol could be required for the commitment of PreMel to the epidermal lineage. In fact, *TGF- β 1* transcript levels also decrease after 4 weeks along with *IL-6*, another cytokine described as an inhibitor of melanin synthesis [75]. Additionally, *CD73* (ecto-5'-nucleotidase) is another classic positive marker of ADSC, and there is no clear correlation between its diminished expression in PreMel and HEM, because there are few reports of *CD73* in normal HEM. *CD73* is a target of *TGF- β* signaling in immune cells (murine *CD4*⁺ T and *CD8*⁺ T cells, dendritic cells, and macrophages) [76] and the reduced signaling of this pathway in PreMel due to the lower *TGF- β 1* expression, and *CD105* levels could be responsible for the decrease in *CD73* expression.

The similarities in the expression of *CD105* and *CD73* between PreMel and HEM, and the functional consequences that may result in diminished signaling by the *TGF- β* pathway for the absence of *CD105*, lead us to propose that *CD105*^{neg} *CD73*^{low} cells represent a viable alternative to replace the lost HEM in vitiligo. We identify *CD105*^{neg} *CD73*^{low} as a heterogeneous cell population expressing *MITF*, *TYR*, and *PMEL* composed of (1) ADSC deriving from the MSC lineage but with functional properties allowing for differentiation and immunomodulation and (2) PreMel with a precursor-like phenotype and the potential to mature into HEM, both of which located at the niche of the epidermis could play a dual role in the treatment of vitiligo: ADSC playing a

regulator function against the inflammatory environment of the pathological skin, and PreMel providing a source of melanin-producing cells that could reach a terminal differentiation in response to components of the microenvironment.

Indeed, ADSC have been used in vitiligo as a co-adjutant of HEM in vitro and in humans in an autologous cell transplant where it has been reported that a combined injection of both augments the proper settlement of HEM in the grafted area [77]. Interestingly, the use of follicular-derived MSC improves survival of HEM by reducing the inflammation within the treated area [12]. Additionally, it has already been reported that dermal mesenchymal stem cells (DMSC) inhibit the homing of lymphocytes CD8⁺ to the perilesional area in the human skin [78]. Hence, our future investigation will focus on deciphering the effect of partially differentiated ADSC on immunosuppression in the inflammatory environment of patients' skin.

Besides the differentiation yield, temporality is relevant when clinical settings are considered. Our differentiation protocol is 150 days shorter than previously published HEM differentiation methods from MSC [40, 42] and is capable of generating a sufficient number of PreMel cells for possible clinical settings. Starting with a 50-mL sample of lipoaspirate, which requires just one ambulatory procedure, we obtained 9×10^6 cells in primary culture with a differentiation protocol started after four to five subcultures of continuous cell proliferation. Additionally, during the differentiation process, the proliferation continues, resulting in 150 times the initial number of cells. Taking into consideration the accessibility of the autologous cell source and the required short ex vivo procedure, fat tissues could be easily harvested from vitiligo patients for ADSC isolation, differentiation, and transplantation in the depigmented skin areas.

Conclusions

We show in this work a short and scalable protocol for obtaining HEM replacement cells as an alternative for the treatment of vitiligo. An accessible and minimally invasive source for adult stem cells was used allowing the possibility for autologous treatments. However, additional effort is required to drive these cells along the translational pathway. This includes the assessment of possible undesired modification of the cells due to ex vivo manipulation following the established in vitro process. Nevertheless, we believe that PreMel open a new therapeutic window for a disease that has been deferentially referred to as "just a cosmetic issue," and give new hope for vitiligo patients.

Additional files

Additional file 1: Figure S1. ADSC characterization. Expression of classical MSC markers was evaluated by flow cytometry. ADSC are positive for (A) CD105, (B) CD90, (C) CD73, (D) CD44, and (E) CD13. Additionally, ADSC are negative for (F) CD31, (G) CD14, (H) CD45, and (I) CD106. (J) CD34 was partially positive as has been described for ADSC. Autofluorescence controls are shown in blue. ADSC have the potential to differentiate into (K) chondrogenic lineage, stained with Safranin O; (L) osteogenic lineage, with Alizarin Red S positive staining; and (M) adipogenic lineage, with cells positive for Oil Red O stain. (Scale bar = 100 μ m). (N) Clonogenic potential of ADSC measured by CFU-F. Colonies composed of more than 50 cells, in 5 dilutions, were quantified. Absorbance of total CV staining was also graphed, $n = 3$. (JPG 2140 kb)

Additional file 2: Figure S2. Gating strategy for flow cytometry analysis. We show representative plots for CD105 expression after the gating of ADSC, PreMel and HEM in the SSC-A vs FSC-A graph, as well as the posterior elimination of doublets. (JPG 820 kb)

Additional file 3: Figure S3. Expression of MSC-related markers. A) Dot plot shows CD44 expression in ADSC, PreMel and HEM. B) MFI ratio for CD44. C) Expression of CD90. D) MFI ratio for CD90. E) Expression of CD146. F) MFI ratio for CD146. G) Expression of CD117. H) MFI ratio for CD117. MFI ratio was calculated as MFI (specific staining)/ MFI (autofluorescence) for each marker. Data from PreMel and HEM were normalized with respect to undifferentiated ADSC. For dot plots, gray dots represent autofluorescence control and black dots represent stained cells with their respective marker $n = 3$, * $P < 0.05$ One-way ANOVA. (JPG 168 kb)

Additional file 4: Figure S4. Reduction of the adipogenic differentiation potential in PreMel. ADSC and PreMel were stimulated for adipogenic differentiation. Red Oil O staining in A) ADSC and B) PreMel. C) Oil Red O⁺ cells quantification shows that the adipose potential is diminished in PreMel respect to ADSC. Scale bar = 500 μ m. * $P < 0.05$ unpaired Student's t test. (JPG 941 kb)

Additional file 5: Fig. S5. Gene expression of HEM-related genes. *SOX2*, *SOX10*, *PAX3*, *MITF-A*, *MITF-M*, *MCTR*, *PMEL*, *TRP2*, *TYR*, and *MLANA* were evaluated in A) HEM and B) A375 cells, an amelanotic melanoma cell line. (JPG 399 kb)

Additional file 6: Figure S6. MITF expression in PreMel and HEM. A) Representative image of MITF immunofluorescence in PreMel shows that the entire population expresses the protein. B) The same result was obtained through cell cytometry analysis. MITF expression in HEM by C) immunofluorescence and D) cell cytometry. Scale bar = 100 μ m. (JPG 453 kb)

Additional file 7: Figure S7. PreMel show similar cell proliferation and stress resistance compared to HEM. A) Growth curve of ADSC, PreMel and HEM shows that the PreMel growth pattern is similar to that of HEM. PDT (population doubling time) and GR (growth rate) were estimated from the data in (A). Cells were exposed to UVR and PDT was estimated during the exponential growth phase. B) A lower PDT in PreMel than in HEM indicates that ADSC are more resistant to UVB radiation. The PDTs of PreMel and HEM are not different after irradiation with 10 or 20 mJ/cm². ADSC have the highest growth rate, whereas PreMel' is lower and similar to that of HEM ($n = 3$, * $P < 0.05$ One-way ANOVA). C) ADSC are sensitive to ROS in all concentrations. At low concentrations of H₂O₂, PreMel and ADSC show similar resistance ($n = 3$, * $P < 0.05$ two-way ANOVA). (JPG 720 kb)

Additional file 8: Figure S8. Levels of whitening-related cytokines. *IL-6* and *TGF- β 1* levels were evaluated after the 4-week differentiation protocol; they are diminished compared to undifferentiated ADSC. (JPG 263 kb)

Abbreviations

ADSC: Adipose-derived stem cells; HEM: Human epidermal melanocytes; MITF: Microphthalmia-associated basic helix-loop-helix leucine zipper transcription factor; MSC: Mesenchymal stem cells; PreMel: Pre-melanocytes; TYR: Tyrosinase

Acknowledgements

We would like to thank Dr. Pablo Contreras and his team at the WLK Clinic for their help in the procurement of adipose tissue samples. Thanks to Macarena Ocaña and Claudia Rubi from Cells for Cells Animal Facility for their assistance in the animal experiments. Thanks to Andrés Ramírez from Cell Cytometry Facility for their help with data analysis and scientific advice. Thanks to Gianna Garza for their valuable help with the revision of this manuscript.

Authors' contributions

GZ and MK were responsible for the conception and design and data analysis. GZ, CS, DM, and RC were responsible for the collection of data. WG was responsible for the sample collection coordination. GZ and MK were responsible for the manuscript writing. All authors read and approved the final manuscript. MK confirms that he had access to all data and supports the submission of this article.

Funding

We would like to thank Consorcio REGENERO, a Chilean Biotechnology Company, for funding cell therapy development.

Availability of data and materials

The datasets analyzed during the current study are available from the corresponding author on reasonable request.

Ethics approval and consent to participate

All the procedures presented in this work were approved by the Ethics Committee of Universidad de los Andes. AT samples were obtained with the informed consent of donors.

Consent for publication

Not applicable

Competing interests

GZ and DM receive stipends from Consorcio REGENERO, a Chilean Biotechnology Company, for cell therapy development. MK receives stipends from Cells for Cells, a Chilean Biotechnology Company, for cell therapy development. CS, RC, and WG declare that they have no competing interests.

Author details

¹Consorcio Regenero, La Plaza 2501, Las Condes, Santiago, Chile. ²Laboratory of Nano-Regenerative Medicine, Faculty of Medicine, Universidad de los Andes, Monseñor Álvaro del Portillo 12455, Las Condes, Santiago, Chile. ³Cells for Cells, La Plaza 2501, Las Condes, Santiago, Chile. ⁴Biomedical Research Center (CIB), Faculty of Medicine, Universidad de los Andes, Monseñor Álvaro del Portillo 12455, Las Condes, Santiago, Chile. ⁵Faculty of Medicine, Universidad de los Andes, Monseñor Álvaro del Portillo 12455, Las Condes, Santiago, Chile.

Received: 24 April 2019 Revised: 26 July 2019

Accepted: 29 July 2019 Published online: 09 August 2019

References

- Uong A, Zon LI. Melanocytes in development and cancer. *J Cell Physiol*. 2010;222:38–41.
- Yamaguchi Y, Hearing VJ. Melanocytes and their diseases. *Cold Spring Harb Perspect Med*. 2014;4:1–19.
- Silver DL, Pavan WJ. The origin and development of neural crest-derived melanocytes. From melanocytes to melanoma. Totowa: Humana Press; 2006. p. 3–26.
- Ezzedine K, Eleftheriadou V, Whitton M, van Geel N. Vitiligo. *Lancet*. 2015; 386:74–84.
- Bishnoi A, Parsad D. Clinical and Molecular Aspects of Vitiligo Treatments. *Int. J. Mol. Sci*. 2018;19. <https://www.mdpi.com/1422-0067/19/5/1509>
- Van Geel N, Speeckaert R. Segmental vitiligo. *Dermatol Clin Elsevier Inc*. 2017;35:145–50.
- El-Zawahry BM, Zaki NS, Bassiouny DA, Sobhi RM, Zaghoul A, Khorshied MM, et al. Autologous melanocyte-keratinocyte suspension in the treatment of vitiligo. *J Eur Acad Dermatol Venereol*. 2011;25:215–20.
- Chen Y-F, Yang P-Y, Hu D-N, Kuo F-S, Hung C-S, Hung C-M. Treatment of vitiligo by transplantation of cultured pure melanocyte suspension: analysis of 120 cases. *J Am Acad Dermatol*. 2004;51:68–74.
- Tegta GR, Parsad D, Majumdar S, Kumar B. Efficacy of autologous transplantation of noncultured epidermal suspension in two different dilutions in the treatment of vitiligo. *Int J Dermatol*. 2006;45:106–10.
- Gauthier Y, Benzekri L. Non-cultured epidermal suspension in vitiligo: from laboratory to clinic. *Indian J Dermatology, Venereol Leprol*. 2012;78:59.
- Lagrange S, Montaudié H, Fontas E, Bahadoran P, Lacour J, Passeron T. Comparison of microneedling and full surface erbium laser dermabrasion for autologous cell suspension grafting in nonsegmental vitiligo: a randomized controlled trial. *Br J Dermatol*. 2019;180:1539–40. <https://onlinelibrary.wiley.com/doi/full/10.1111/bjd.17464>.
- Muhammed RT, Kumar R, Rani S, Kumaran SM, Tanwar S, Parsad D. Combination of follicular and epidermal cell suspension as a novel surgical approach in difficult-to-treat vitiligo a randomized clinical trial. *JAMA Dermatol*. 2018;154:301–8.
- Mulekar SV, Al Issa A, Al EA. Treatment of vitiligo on difficult-to-treat sites using autologous noncultured cellular grafting. *Dermatologic Surg*. 2009;35:66–71.
- Redondo P, Gimenez de Azcarate A, Nunez-Cordoba JM, Andreu EJ, Garcia-Guzman M, Aguado L, et al. Efficacy of autologous melanocyte transplantation on amniotic membrane in patients with stable leukoderma: a randomized clinical trial. *JAMA Dermatol*. 2015;151:897–9.
- Verma R, Grewal RS, Chatterjee M, Pragasam V, Vasudevan B, Mitra D. A comparative study of efficacy of cultured versus non cultured melanocyte transfer in the management of stable vitiligo. *Med J Armed Forces India*. 2014;70:26–31.
- Yao L, Zhong S-X, Hu D-N, Guo J-W, Li S-S, Xie X-L, et al. Repigmentation of leukotrichia in vitiligo with transplantation of cultured autologous melanocytes. *Int J Dermatol*. 2014;53:1016–8.
- Ghosh D, Shenoy S, Kuchroo P. Cultured melanocytes: from skin biopsy to transplantation. *Cell Transplant Cognizant Communication Corporation*. 2008;17:351–60.
- Puri N, Mojamdar M, Ramaiah A. Growth defects of melanocytes in culture from vitiligo subjects are spontaneously corrected in vivo in repigmenting subjects and can be partially corrected by the addition of fibroblast-derived growth factors in vitro. *Arch Dermatol Res*. 1989;281:178–84.
- Czajkowski R. Comparison of melanocytes transplantation methods for the treatment of vitiligo. *Dermatol Surg*. 2004;30:1400–5.
- Czajkowski R, Placek W, Drewna T, Kowalyszyn B, Sir J, Weiss W. Autologous cultured melanocytes in vitiligo treatment. *Dermatologic Surg*. 2007;33:1027–35.
- Yamane T, Hayashi S, Mizoguchi M, Yamazaki H, Kunisada T. Derivation of melanocytes from embryonic stem cells in culture. *Dev Dyn*. 1999;216:450–8.
- Fang D, Leishear K, Nguyen TK, Finko R, Cai K, Fukunaga M, et al. Defining the conditions for the generation of melanocytes from human embryonic stem cells. *Stem Cells*. 2006;24:1668–77.
- Motohashi T, Aoki H, Yoshimura N, Kunisada T. Induction of melanocytes from embryonic stem cells and their therapeutic potential. *Pigment Cell Res*. 2006;19:284–9.
- Yang R, Zheng Y, Li L, Liu S, Burrows M, Wei Z, et al. Direct conversion of mouse and human fibroblasts to functional melanocytes by defined factors. *Nat Commun*. 2014;5:5807.
- Mica Y, Lee G, Chambers SM, Tomishima MJ, Studer L. Modeling neural crest induction, melanocyte specification, and disease-related pigmentation defects in hESCs and patient-specific iPSCs. *Cell Rep The Authors*. 2013;3:1140–52.
- Nissan X, Larribere L, Saidani M, Delevoye C, Feteira J, Lemaitre G, et al. Correction for Nissan et al., Functional melanocytes derived from human pluripotent stem cells engraft into pluristratified epidermis. *Proc Natl Acad Sci*. 2011;108:17856.
- Ohta S, Imaizumi Y, Okada Y, Akamatsu W, Kuwahara R, Ohyama M, et al. Generation of human melanocytes from induced pluripotent stem cells. *PLoS One*. 2011;6:e16182.
- Gledhill K, Guo Z, Umegaki-Arao N, Higgins CA, Itoh M, Christiano AM. Melanin transfer in human 3D skin equivalents generated exclusively from induced pluripotent stem cells. *PLoS One*. 2015;10:e0136713.
- Yamauchi T, Yamasaki K, Tsuchiyama K, Koike S, Aiba S. A quantitative analysis of multilineage-differentiating stress-enduring (Muse) cells in human adipose tissue and efficacy of melanocytes induction. *J Dermatol Sci*. 2017;86:198–205.

30. Tsuchiyama K, Wakao S, Kuroda Y, Ogura F, Nojima M, Sawaya N, et al. Functional melanocytes are readily reprogrammable from multilineage-differentiating stress-enduring (muse) cells, distinct stem cells in human fibroblasts. *J Invest Dermatol*. 2013;133:2425–35.
31. Medvedev SP, Shevchenko AI, Zakian SM. Induced pluripotent stem cells: problems and advantages when applying them in regenerative medicine. *Acta Naturae. Natl Res University Higher School Econ*. 2010;2:18–28.
32. Martin U. Therapeutic application of pluripotent stem cells: challenges and risks. *Front Med*. 2017;4:229.
33. Kolf CM, Cho E, Tuan RS. Mesenchymal stromal cells. Biology of adult mesenchymal stem cells: regulation of niche, self-renewal and differentiation. *Arthritis Res Ther*. 2007;9:204.
34. Uccelli A, Moretta L, Pistoia V. Mesenchymal stem cells in health and disease. *Nat Rev Immunol*. 2008;8:726–36.
35. Ma S, Xie N, Li W, Yuan B, Shi Y, Wang Y. Immunobiology of mesenchymal stem cells. *Cell Death Differ*. 2014;21:216–25.
36. Gimble JM, Guilak F, Nuttall ME, Sathishkumar S, Vidal M, Bunnell BA. In vitro differentiation potential of mesenchymal stem cells. *Transfus Med Hemother*. 2008;35:228–38.
37. Pittenger MF, Mackay AM, Beck SC, Jaiswal RK, Douglas R, Mosca JD, et al. Multilineage potential of adult human mesenchymal stem cells. *Science (80-)*. 2011;143:143–7.
38. Lalu MM, McIntyre L, Pugliese C, Fergusson D, Winston BW, Marshall JC, et al. Safety of cell therapy with mesenchymal stromal cells (SafeCell): a systematic review and meta-analysis of clinical trials. *PLoS One*. 2012;7:e47559.
39. Bartolucci J, Verdugo FJ, González PL, Larrea RE, Abarzua E, Goset C, et al. Safety and efficacy of the intravenous infusion of umbilical cord mesenchymal stem cells in patients with heart failure: a phase 1/2 randomized controlled trial (RIMECARD Trial [Randomized Clinical Trial of Intravenous Infusion Umbilical Cord Mesenchymal]). *Circ Res* 2017;121:1192–1204.
40. Paino F, Ricci G, De Rosa A, D'Aquino R, Laino L, Pirozzi G, et al. Ecto-mesenchymal stem cells from dental pulp are committed to differentiate into active melanocytes *Eur Cell Mater* 2010;20:295–305.
41. Stevens A, Zuliani T, Olejnik C, LeRoy H, Obriot H, Kerr-Conte J, et al. Human dental pulp stem cells differentiate into neural crest-derived melanocytes and have label-retaining and sphere-forming abilities. *Stem Cells Dev*. 2008;17:1175–84.
42. Mei X, Sun Y, Wu Z, Pan W, Zhu J, Shi W. In vitro-induced differentiation of bone marrow mesenchymal stem cells into melanocytes. *Cell Biol Int*. 2015;39:824–33.
43. Kim J-Y, Do PC, Lee JH, Lee C-H, Do B-R, Lee AY. Co-culture of melanocytes with adipose-derived stem cells as a potential substitute for co-culture with keratinocytes. *Acta Derm Venereol*. 2012;92:16–23.
44. Lim WS, Kim CH, Kim JY, Do BR, Kim EJ, Lee AY. Adipose-Derived Stem Cells Improve Efficacy of Melanocyte Transplantation in Animal Skin. *Biomol Ther (Seoul)*. 2014;22:328–33. <http://www.biomolther.org/journal/view.html?volume=22&number=4&spage=328&year=2014>.
45. Zuk PA, Zhu M, Ashjian P, De Ugarte DA, Huang JI, Mizuno H, et al. Human adipose tissue is a source of multipotent stem cells. *Mol Biol Cell*. 2002;13:4279–95.
46. Dominici M, Le Blanc K, Mueller I, Slaper-Cortenbach I, Marini F, Krause DS, et al. Minimal criteria for defining multipotent mesenchymal stromal cells. The International Society for Cellular Therapy position statement. *Cytotherapy*. 2006;8:315–7.
47. Bourin P, Bunnell BA, Casteilla L, Dominici M, Katz AJ, March KL, et al. Stromal cells from the adipose tissue-derived stromal vascular fraction and culture expanded adipose tissue-derived stromal/stem cells: a joint statement of the International Federation for Adipose Therapeutics and Science (IFATS) and the International So. *Cytotherapy*. 2013;15:641–8.
48. Pan T, Zhu J, Hwu W-J, Jankovic J. The role of alpha-synuclein in melanin synthesis in melanoma and dopaminergic neuronal cells. *PLoS One*. 2012;7:e45183.
49. Alexeev V, Yoon K. Distinctive role of the cKit receptor tyrosine kinase signaling in mammalian melanocytes. *J Invest Dermatol*. 2006;126:1102–10.
50. Yamamoto H, Yamane T, Iguchi K, Tanaka K, Iddamalgoda A, Unno K, et al. Melanin production through novel processing of proopiomelanocortin in the extracellular compartment of the auricular skin of C57BL/6 mice after UV-irradiation. *Sci Rep*. 2015;5:1–11.
51. Udono T, Yasumoto K, Takeda K, Amae S, Watanabe K, Saito H, et al. Structural organization of the human microphthalmia-associated transcription factor gene containing four alternative promoters. *Biochim Biophys Acta*. 2000;1491:205–19.
52. Du J, Miller AJ, Widlund HR, Horstmann MA, Ramaswamy S, Fisher DE. MLANA/MART1 and SILV/PMEL17/GP100 are transcriptionally regulated by MITF in melanocytes and melanoma. *Am J Pathol*. 2003;163:333–43.
53. Olivares C, Solano F, García-Borrón JC. Conformation-dependent post-translational glycosylation of tyrosinase: requirement of a specific interaction involving the CuB metal binding site. *J Biol Chem Am Soc Biochem Mol Biol*. 2003;278:15735–43.
54. Coleman DL. Effect of genic substitution on the incorporation of tyrosine into the melanin of mouse skin. *Arch Biochem Biophys*. 1962;96:562–8.
55. Dong L, Li Y, Cao J, Liu F, Pier E, Chen J, et al. FGF2 regulates melanocytes viability through the STAT3-transactivated PAX3 transcription. *Cell Death Differ*. 2012;19:616–22.
56. Hirobe T. Basic fibroblast growth factor stimulates the sustained proliferation of mouse epidermal melanoblasts in a serum-free medium in the presence of dibutyryl cyclic AMP and keratinocytes. *Development*. 1992;114:435–45.
57. Ekerbicer N, Inan S, Tarakci F, Zeren T. The effects of DBcAMP on the expression of eNOS, iNOS and TGF-beta in rat heart tissue. *Biotech Histochem*. 2009;84:47–54.
58. Hirobe T. Keratinocytes regulate the function of melanocytes. *Dermatologica Sin*. 2014;32:200–4.
59. Rosner BA, Cristofalo VJ. Hydrocortisone: a specific modulator of in vitro cell proliferation and aging. *Mech Ageing Dev*. 1979;9:485–96.
60. Hirobe T. Hydrocortisone is involved in regulating the proliferation and differentiation of mouse epidermal melanoblasts in serum-free culture in the presence of keratinocytes. *Eur J Cell Biol*. 1996;71:387–94.
61. Pittelkow MR, Shipley GD. Serum-free culture of normal human melanocytes: growth kinetics and growth factor requirements. *J Cell Physiol*. 1989;140:565–76.
62. Sun Q, Rabbani P, Takeo M, Lee S-H, Lim CH, Noel E-NS, et al. Dissecting Wnt signaling for melanocyte regulation during wound healing. *J Invest Dermatol*. 2018;138:1591–600.
63. Saldana-Caboverde A, Kos L. Roles of endothelin signaling in melanocyte development and melanoma. *Pigment Cell Melanoma Res*. 2010;23:160–70.
64. Epstein DJ, Vekemans M, Gros P. splotch (Sp2H), a mutation affecting development of the mouse neural tube, shows a deletion within the paired homeodomain of Pax-3. *Cell*. 1991;67:767–74.
65. Blake JA, Ziman MR. Pax3 transcripts in melanoblast development. *Develop Growth Differ*. 2005;47:627–35.
66. Watanabe A, Takeda K, Ploplis B, Tachibana M. Epistatic relationship between Waardenburg syndrome genes MITF and PAX3. *Nat Genet*. 1998;18:283–6.
67. Amae S, Fuse N, Yasumoto K, Sato S, Yajima I, Yamamoto H, et al. Identification of a novel isoform of microphthalmia-associated transcription factor that is enriched in retinal pigment epithelium. *Biochem Biophys Res Commun*. 1998;247:710–5.
68. Galibert MD, Yavuzer U, Dexter TJ, Goding CR. Pax3 and regulation of the melanocyte-specific tyrosinase-related protein-1 promoter. *J Biol Chem. Am Soc Biochem Mol Biol*. 1999;274:26894–900.
69. Wolf Horrell EM, Boulanger MC, D'Orazio JA. Melanocortin 1 receptor: structure, function, and regulation. *Front Genet*; 2016;7:95.
70. Swope VB, Jameson JA, McFarland KL, Supp DM, Miller WE, McGraw DW, et al. Defining MC1R regulation in human melanocytes by its agonist α -melanocortin and antagonists agouti signaling protein and B-defensin 3. *J Invest Dermatol*. 2012;132:2255–62.
71. Donatien PD, Hunt G, Pieron C, Lunec J, Tåleb A, Thody AJ. The expression of functional MSH receptors on cultured human melanocytes. *Arch Dermatol Res*. 1992;284:424–6.
72. Martínez-Esparza M, Solano F, García-Borrón JC. Independent regulation of tyrosinase by the hypopigmenting cytokines TGF beta1 and TNF alpha and the melanogenic hormone alpha-MSH in B16 mouse melanocytes. *Cell Mol Biol (Noisy-le-grand)*. 1999;45:991–1000.
73. Jung H, Kim HH, Lee DH, Hwang YS, Yang HC, Park JC. Transforming growth factor-beta 1 in adipose derived stem cells conditioned medium is a dominant paracrine mediator determines hyaluronic acid and collagen expression profile. *Cytotechnol*. 2011;63:57–66.
74. Martínez-Esparza M, Jiménez-Cervantes C, Beermann F, Aparicio P, Lozano JA, García-Borrón JC. Transforming growth factor- β 1 inhibits basal melanogenesis in B16/F10 mouse melanoma cells by increasing the rate of

- degradation of tyrosinase and tyrosinase-related protein-1. *J Biol Chem. Am Soc Biochem Mol Biol*; 1997;272:3967–3972.
75. Kim D-W, Jeon B-J, Hwang N-H, Kim M-S, Park S-H, Dhong E-S, et al. Adipose-derived stem cells inhibit epidermal melanocytes through an interleukin-6-mediated mechanism. *Plast Reconstr Surg*. 2014;134:470–80.
 76. Regateiro FS, Howie D, Nolan KF, Agorogiannis EI, Greaves DR, Cobbold SP, et al. Generation of anti-inflammatory adenosine by leukocytes is regulated by TGF- β . *Eur J Immunol*. 2011;41:2955–65.
 77. Saleh AA, Salam OHA, Metwally GH, Abdelsalam HA, Hassan MA, et al. Comparison Treatment of Vitiligo by Co-culture of Melanocytes Derived from Hair Follicle with Adipose-Derived Stem Cells with and without NB-UVB. *Pigmentary Disorders*. 2017;4:256. <https://www.omicsonline.org/open-access/comparison-treatment-of-vitiligo-by-coculture-of-melanocytes-derived-from-hair-follicle-with-adiposederived-stem-cells-with-and-wi-2376-0427-1000256.php?aid=86078>.
 78. Zhou MN, Zhang ZQ, Wu JL, Lin FQ, Fu LF, Wang SQ, et al. Dermal mesenchymal stem cells (DMSCs) inhibit skin-homing CD8+ T cell activity, a determining factor of vitiligo patients' autologous melanocytes transplantation efficiency. *PLoS One*. 2013;8:1–10.

Publisher's Note

Springer Nature remains neutral with regard to jurisdictional claims in published maps and institutional affiliations.

Ready to submit your research? Choose BMC and benefit from:

- fast, convenient online submission
- thorough peer review by experienced researchers in your field
- rapid publication on acceptance
- support for research data, including large and complex data types
- gold Open Access which fosters wider collaboration and increased citations
- maximum visibility for your research: over 100M website views per year

At BMC, research is always in progress.

Learn more biomedcentral.com/submissions

